Computational Energy Science

Vol. 3, No. 1, p. 14-17, 2026

Original article

Phonon-informed interfacial adsorption modeling for natural hydrogen recovery and CO_2-enhanced recovery

Duxue Wang[1]*

[1]College of New Energy, China University of Petroleum (East China), Qingdao 266000, P. R. China

Keywords:
Natural hydrogen
phonon calculation
competitive adsorption
CO_2-enhanced recovery
pore-network modeling
adsorbed-layer thickness

Cited as:
Wang, D. Phonon-informed interfacial adsorption modeling for natural hydrogen recovery and CO_2-enhanced recovery. Computational Energy Science, 2026, 3(1): 14-17.
https://doi.org/10.46690/compes.2026.01.03

Abstract:
Natural (geologic) hydrogen is a potential carbon-free energy resource, but its subsurface storage and recovery depend on multicomponent adsorption within nanoscale pores. We developed a phonon-informed upscaling framework that links adsorption energetics to pore-network transport parameters. A diatomic normal-mode model was used to quantify adsorption energy and the adsorption-bond force constant for H_2, N_2, CH_4, and CO_2 on quartz. These quantities were combined with a van't Hoff equilibrium relation and a Langmuir isotherm to calculate a temperature and pressure-dependent adsorbed-layer thickness, $\delta(T,P)$, replacing the conventional fixed-thickness assumption. The adsorption energies followed CO_2 (0.28 eV) > CH_4 (0.15 eV) > N_2 (0.12 eV) > H_2 (0.08 eV), with corresponding force constants of 73.2, 39.2, 31.4, and 20.9 $N\,m^{-1}$. At 350 K, the calculated CO_2/N_2 adsorption selectivity was 758, indicating favorable competitive displacement of adsorbed hydrogen by injected CO_2. The state-dependent adsorbed layers reduced the effective pore radius and modified throat conductance and capillary entry pressure. This framework provides an experimentally calibratable route for transferring interfacial vibrational information into reservoir-scale models of natural hydrogen production and CO_2 sequestration.

1. Introduction

Natural hydrogen is generated and accumulated in the subsurface through processes that include serpentinization, radiolysis, and deep degassing (Zgonnik, 2020; Novella et al., 2024). It has attracted interest as a potentially abundant carbon-free energy resource. Unlike manufactured hydrogen, geologic hydrogen does not require an upstream conversion step before extraction. Its recovery, however, depends on interfacial processes that also govern conventional and unconventional gas reservoirs. Hydrogen interacts weakly with mineral surfaces, and this interaction affects storage, transport, and producibility (Zhang et al., 2026).

Hydrogen is the lightest and smallest molecule and adsorbs weakly on many mineral surfaces. Coexisting gases, including methane, nitrogen, and especially carbon dioxide, can adsorb more strongly. This contrast has two practical consequences. Strong adsorption by coexisting gases reduces the effective pore volume available for hydrogen flow. The same contrast may also enable CO_2-enhanced hydrogen recovery (CO_2-EHGR), in which injected CO_2 competitively displaces adsorbed hydrogen while remaining in the subsurface. This concept is analogous to CO_2-enhanced shale-gas recovery (Liu et al., 2022).

Adsorbed-layer thickness is a key interfacial parameter because it determines the effective pore radius and associated transport coefficients. Many pore-network and continuum models treat this thickness as a constant. For example, the physics-consistent upscaling workflow of Liu et al. (2026) evaluated fixed values of 0 and 1 nm. A fixed value cannot represent the temperature and pressure dependence of adsorption and introduces uncertainty into reservoir simulations.

This study establishes a phonon-informed parameter-transfer pathway for natural hydrogen systems. Adsorption energy and adsorption-bond stiffness are related to the normal modes of an adsorbate-surface system. The resulting energetics are transferred through a van't Hoff equilibrium relation and

*Corresponding author.
E-mail address: 15670982709@163.com (D. Wang).

Yandy Scientific Press

3007-5602 © The Author(s) 2024.
Received January 12, 2026; revised February 11, 2026; accepted March 15, 2026; available online March 20, 2026.

a Langmuir isotherm to calculate state-dependent adsorbed layers. The framework is applied to H_2, N_2, CH_4, and CO_2 on quartz. We then quantify competitive adsorption, evaluate CO_2-EHGR selectivity, and propagate the adsorbed-layer thickness into pore-network transport parameters.

2. Methods

2.1 Phonon based adsorption Energetics

Adsorption on quartz was represented by a diatomic normal-mode model. A surface oxygen atom of mass m_s was connected to the substrate by a spring with force constant k_s. An adsorbed molecule of mass m_a was connected to the surface atom by a weaker spring with force constant k_a. The bare-surface frequency was assigned to the quartz Si-O stretching mode at 1,050 cm^{-1}, from which k_s was calculated.

The adsorption-bond force constant was defined as the curvature of a Morse adsorption potential at its equilibrium position. With a characteristic physisorption-well width of approximately 0.35 Å, the relation is:

$$k_a = V''(r_e) = \frac{2E_{\text{ads}}}{\delta_a^2} \tag{1}$$

where E_{ads} is the adsorption energy, δ_a is the characteristic well width, and r_e is the equilibrium separation. The coupled surface-adsorbate system was described by the force-constant and mass matrices:

$$\mathbf{K} = \begin{bmatrix} k_s + k_a & -k_a \\ -k_a & k_a \end{bmatrix}, \quad \mathbf{M} = \text{diag}(m_s, m_a) \tag{2}$$

The mass-weighted Hessian, $\mathbf{F} = \mathbf{M}^{-1/2}\mathbf{K}\mathbf{M}^{-1/2}$, was diagonalized to obtain the two normal-mode frequencies. Because k_s was much larger than k_a, the low-frequency mode represented the adsorption-bond vibration, $\omega_{\text{ads}} \approx \sqrt{k_a/m_a}$. This frequency can be calibrated against vibrational spectroscopy measurements.

2.2 State dependent adsorbed layer thickness

The adsorbed-layer thickness was calculated from a Langmuir isotherm with a van't Hoff temperature dependence for the equilibrium constant:

$$\delta_{ads}(T,P) = \delta_{max}\frac{K(T)P}{1+K(T)P}, \quad K(T) = K_0 \exp\left(\frac{E_{ads}}{k_B T}\right) \tag{3}$$

Here, δ_{max} is the maximum monolayer thickness and was set to 1.2 nm. The prefactor K_0 was calibrated separately for each species to reproduce its reference thickness at 350 K and 10 MPa. This formulation replaces a fixed adsorbed layer with a continuous function of reservoir temperature and pressure.

2.3 Competitive adsorption selectivity

For two gases i and j that follow Langmuir adsorption, selectivity was calculated as the ratio of their equilibrium constants:

$$S_{ij} = \frac{K_i}{K_j} = \exp\left(\frac{E_{\text{ads},i} - E_{\text{ads},j}}{k_B T}\right) \tag{4}$$

The selectivity therefore depends on the adsorption-energy difference and provides a thermodynamic measure of competitive displacement.

2.4 Pore network transport upscaling

The adsorbed layer reduced the effective throat radius according to $r_{\text{eff}} = r_t - \delta_{\text{ads}}$. Following the pore-network formulation of Liu et al. (2026), throat conductance and capillary entry pressure were calculated as:

$$g_t = \frac{\pi r_{eff}^4}{8\mu L}\left(1 + \frac{4b}{r_{eff}}\right), \quad p_c = \frac{2\gamma\cos\theta}{r_{eff}} \tag{5}$$

where μ is the phase viscosity, L is the throat length, b is the slip length, γ is the interfacial tension, and θ is the contact angle. Because conductance scales strongly with effective radius, small changes in the adsorbed layer can produce appreciable transport changes. The representative calculations used a 5.0 nm throat radius and a 5.0 nm slip length.

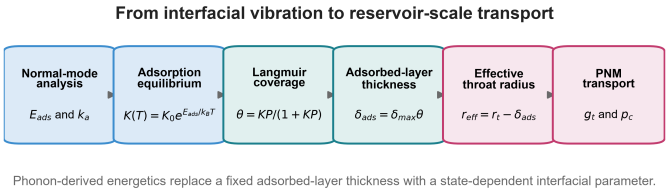


Fig. 1. Phonon-informed interfacial upscaling workflow. Normal-mode analysis yields adsorption energetics, which determine the equilibrium constant, Langmuir coverage, adsorbed-layer thickness, effective throat radius, and pore-network transport parameters.

3. Results

3.1 Adsorption energetics

Fig. 2 illustrates the physical distinction between weak hydrogen adsorption and preferential carbon-dioxide adsorption within a quartz nanopore. Table 1 and Fig. 3 summarize the calculated adsorption energetics for all four gases.

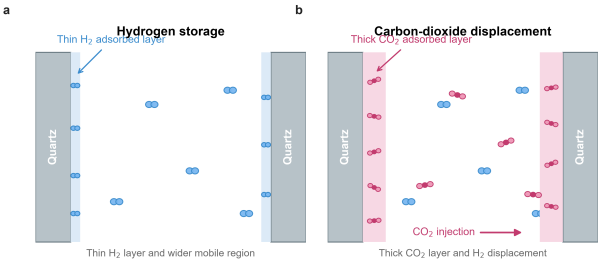


Fig. 2. Conceptual comparison of hydrogen storage and carbon-dioxide displacement in a quartz nanopore. (a) Weak hydrogen adsorption produces a thin layer and wider mobile region. (b) Preferential carbon-dioxide adsorption displaces hydrogen and forms a thicker interfacial layer. Molecule counts are illustrative.

Table 1. Phonon-derived adsorption parameters on quartz at 350 K and 10 MPa.

Species	Adsorption energy (eV)	Force constant (Nm^{-1})	Vibrational frequency (cm^{-1})	Layer thickness (nm)
H_2	0.08	20.9	414.8	0.20
N_2	0.12	31.4	135.8	0.35
CH_4	0.15	39.2	199.9	0.45
CO_2	0.28	73.2	162.3	0.60

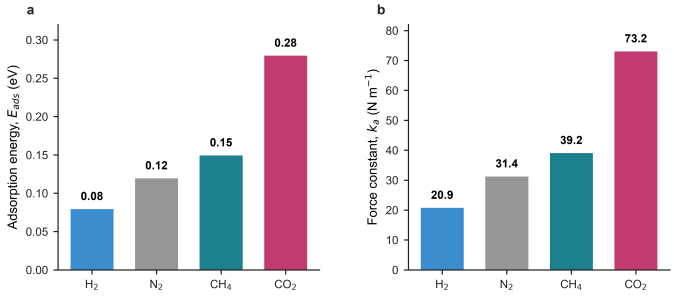


Fig. 3. Phonon-derived adsorption energetics on quartz. (a) Adsorption energies and (b) adsorption-bond force constants for H_2, N_2, CH_4, and CO_2.

Adsorption energy increased from 0.08 eV for H_2 to 0.28 eV for CO_2. The adsorption-bond force constant increased from 20.9 Nm^{-1} for H_2 to 73.2 Nm^{-1} for CO_2. The calculated adsorption-strength order was $CO_2 > CH_4 > N_2 > H_2$.

3.2 Emperature and pressure effects on the adsorbed layer

The adsorbed-layer thickness decreased with temperature and increased with pressure for all four gases (Fig. 4). At 350 K and 10 MPa, the hydrogen layer was 0.20 nm and the carbon-dioxide layer was 0.60 nm. Carbon dioxide retained the thickest layer across the pressure range examined.

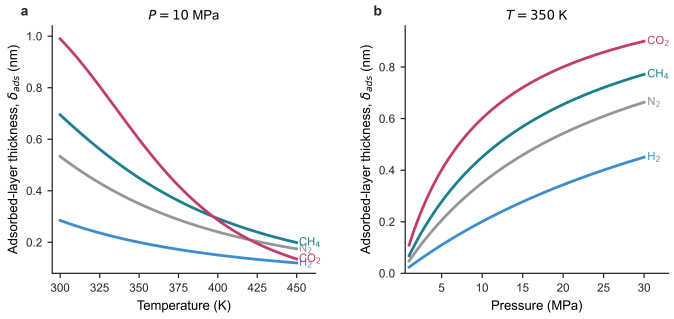


Fig. 4. State dependence of the adsorbed-layer thickness. (a) Temperature dependence at 10 MPa. (b) Pressure dependence at 350 K. Curves were calculated with the van't Hoff-Langmuir formulation and the reference values in Table 1.

3.3 Competitive adsorption and carbon dioxide selectivity

Carbon dioxide was strongly favored over the other gases across the temperature range examined (Fig. 5(a)) At 350 K, the CO_2/H_2 selectivity was 758, compared with 201 for CO_2/N_2 and 74 for CO_2/CH_4. The largest selectivity resulted from the 0.20 eV adsorption-energy difference between CO_2 and H_2.

3.4 Consequences for pore scale transport

The hydrogen adsorbed layer produced continuous temperature-dependent changes in throat conductance and capillary entry pressure (Fig. 6). Conductance increased as thermal desorption widened the effective throat. Capillary entry pressure decreased over the same temperature range. The fixed no-adsorption assumption did not reproduce either trend.

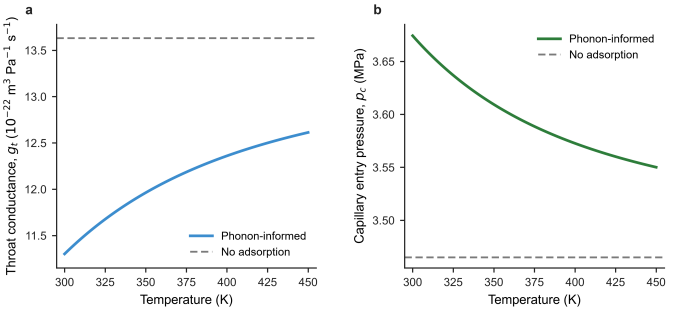


Fig. 6. Temperature dependence of hydrogen-phase transport parameters. (a) Throat conductance and (b) capillary entry pressure from the phonon-informed adsorbed-layer model. Dashed lines denote the no-adsorption reference for a 5.0 nm throat.

4. Discussion

The energetic ordering is consistent with weak physisorption of nonpolar H_2 and stronger interaction of quadrupolar CO_2 with quartz. The corresponding force constant provides a sharper measure of adsorption-potential curvature than the well depth alone. Its associated vibrational frequency also offers a possible connection between the model and spectroscopic calibration.

The high CO_2/H_2 selectivity indicates that injected CO_2 can preferentially occupy adsorption sites and displace hydrogen. This thermodynamic advantage supports the feasibility of CO_2-EHGR and creates a potential route for simultaneous CO_2 retention. The geometric response introduces a counteracting effect. A thicker CO_2 layer narrows the mobile pore region and can reduce effective permeability. Injection design must therefore balance competitive displacement against adsorption-induced flow restriction.

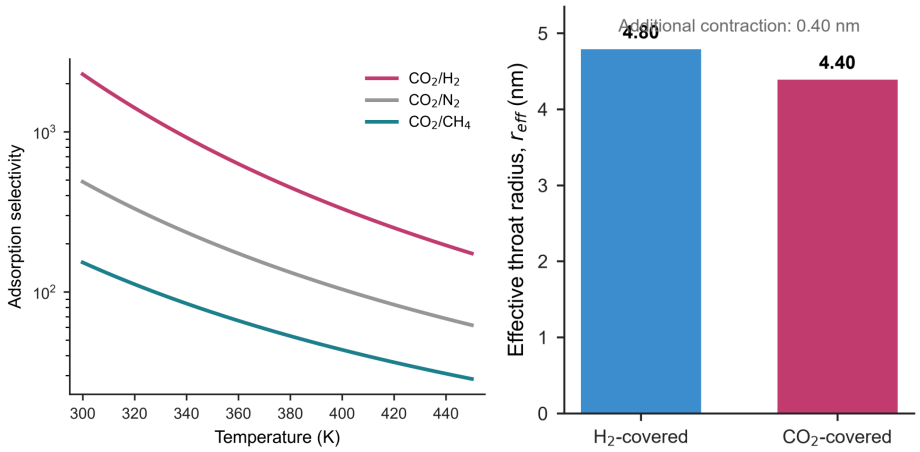


Fig. 5. Competitive adsorption and pore-throat contraction. (a) CO_2 adsorption selectivity relative to H_2, N_2, and CH_4. (b) Effective radius of a 5.0 nm throat with the H_2 or CO_2 adsorbed layer at 350 K and 10 MPa.

The results are model predictions for a representative quartz surface. The formulation assumes a single-site Langmuir isotherm, a prescribed maximum monolayer thickness, and idealized pore geometry. Mineral heterogeneity, surface water, reactive transport, and multicomponent nonideality were not resolved. Experimental adsorption and vibrational measurements are therefore needed before reservoir-scale application.

5. Conclusions

A phonon-informed upscaling framework was developed to connect interfacial adsorption energetics with pore-network transport in natural hydrogen systems. Calculations for H_2, N_2, CH_4, and CO_2 on quartz gave the adsorption-strength order $CO_2 > CH_4 > N_2 > H_2$. The van't Hoff-Langmuir relation converted these energetics into temperature- and pressure-dependent adsorbed-layer thicknesses. At 350 K, the predicted CO_2/H_2 selectivity was 758, supporting preferential displacement of adsorbed hydrogen by CO_2. For a 5.0 nm throat at the reference conditions, the H_2 and CO_2 layers produced effective radii of 4.80 and 4.40 nm. The framework therefore captures both the displacement benefit of CO_2 injection and the associated flow restriction. Experimental calibration and extension to heterogeneous, water-bearing mineral surfaces are required for reservoir-scale prediction.

Acknowledgements

This work was supported by the Shandong Excellent Young Scientist (Overseas) Program (No. 2024HWYQ-050).

Conflict of interest

The author declares no competing interest.

Open Access This article is distributed under the terms and conditions of the Creative Commons Attribution (CC BY-NC-ND) license, which permits unrestricted use, distribution, and reproduction in any medium, provided the original work is properly cited.

References

Liu, J., Zhang, T., Sun, S. Mechanism analysis of shale gas adsorption under carbon dioxide-moisture conditions: A molecular dynamic study. Energy & Fuels, 2022, 36(24): 14865-14873.

Liu, J., Wang, K., Song, H., et al. Porous media flow modeling from molecular simulations to pore-network modeling: Physics-consistent upscaling of interfacial transport parameters. Computational Geosciences, 2026, 30(15).

Langmuir, I. The adsorption of gases on plane surfaces of glass, mica and platinum. Journal of the American Chemical Society, 1918, 40 (9): 1361-1403.

Novella, D., Demouchy, S., Bolfan-Casanova, N. Deep hydrogen reservoirs and longevity. Elements, 2024, 20(4): 235-240.

Zgonnik, V. The occurrence and geoscience of natural hydrogen: A comprehensive review. Earth-Science Reviews, 2020, 203: 103140.

Zhang, T., He, S., Chen, H., et al. Multiscale energy and mass transport for a sustainable geo-energy future. Advances in Geo-Energy Research, 2026, 20(2): 194-196.